A MECHANISM FOR SELF-EXCITED OSCILLATIONS OF "HAMMERHEAD" AND OTHER BLUNT-NOSE MISSILES

Lars-Eric Ericsson, Phineas Woods and Joseph N. Chavez
Lockheed Missiles and Space Company
A Division of Lockheed Aircraft Corporation
Sunnyvale, California

Abstract

A mechanism for self-excited oscillations at transonic speeds is demonstrated mathematically for missile shapes combining a blunt payload with a flared interstage. Aerodynamic forces are derived on the basis of data obtained for blunt, flared bodies of revolution. Flow separation caused by the blunt payload is assumed to be stable and present at all angles of attack including zero. The flare lift induced by the wake from the nose is generally out of phase with the instantaneous motion of the flare and can cause aeroelastic instability if it is of sufficient magnitude. The phasing is controlled by the shape of the elastic deflection curve, the corresponding bending frequency and the forward velocity of the vehicle. The magnitude of the induced flare lift depends upon the shape of the payload and flare.

Introduction

The appearance of the "hammerhead" missile and other blunt-nose shapes is characterized by the Argos of 1958, the Atlas-Able of 1960 and the various Atlas-Agena vehicles, such as Nimbus and Advent. The word "hammerhead" is used here to indicate a payload whose cross-sectional diameter is larger than that of the adjacent booster. The external shape reflects the economy of using well-tested, and therefore, reliable boosters for an arbitrary payload. The proper design of these vehicles requires an understanding of the aerodynamic forces arising from a complex flow field produced by blunt payloads, conical after-bodies or boat tails and flared interstages all of which form an envelope prescribed by the vehicle's mission and the size of its boosters.

What is offered here is a simple mechanism for producing de-stabilizing aerodynamic forces together with some criteria for controlling the forces. A pre-requisite for the mechanism is a blunt payload together with a flared interstage located at some distance aft of the nose. It is assumed that the payload geometry will cause the flow to separate. A wake is created, as a result, which induces aerodynamic forces at all points on the vehicle aft of the nose. At high subsonic and transonic speeds, the induced lift forces at the flared interstage can be of sufficient magnitude so as to cause self-excited aeroelastic bending oscillations. For some payload shapes, the existence of destabilizing induced forces does not preclude the presence of other types of driving forces. They may exist, for example, simultaneously with buffeting forces which are virtually independent of the vehicle motion. Buffeting forces having a random frequency distribution are reported in (1). In what follows, buffeting of this type is not considered. Instead, attention is focused upon aeroelastic self-excitation arising from the forces induced in the wake of stable flow separation.

The Aerodynamic Forces for Separated Flow at Small Angle of Attack

Static Forces

We begin by considering a blunt nose shape at a small constant angle of attack with flow separation assumed to occur at the payload as indicated in Fig. 1. For simplicity, the lift distribution is approximated by two discrete forces: L_N at the nose and L_F at the flare, separated by the distance b. If the flow were attached over the entire body, the forces L_N and L_F would be determined mainly by the local angle of attack at the nose and at the flare, respectively. Experience shows, however, that with separated flow occurring on blunt, flared bodies of revolution, the interference effects are no longer negligible. In fact, the force on the flare is the sum of two forces; namely,

$$L_F = L(\alpha_F) + \Delta^i L_F \qquad (1)$$

where

α_F = local angle of attack at flare (which for the static case shown here is equal to the angle of attack at the nose, α_N)

$\Delta^i L_F$ = force induced by the wake created at the nose.

The flow field producing the induced lift is generated at the nose and, therefore, mainly determined by the angle of

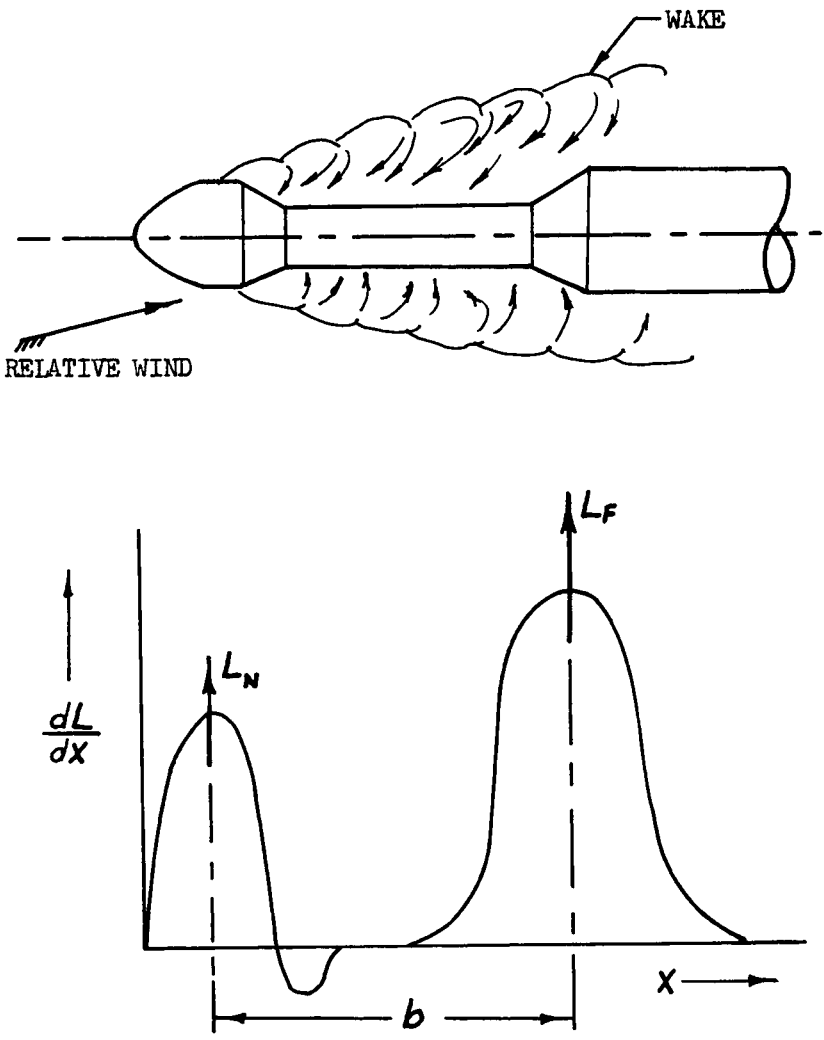

Fig. 1. Force Distribution in Wake of Separated Flow.

attack at the nose. Thus, if the aerodynamic characteristics are linear, the induced lift can be written

$$\Delta^i L_F = \left(\Delta^i L_\alpha\right)_F \cdot \alpha_N$$

Eq. (1) then becomes

$$L_F = \left(L_\alpha\right)_F \cdot \alpha_F + \left(\Delta^i L_\alpha\right)_F \cdot \alpha_N \qquad (2)$$

or

$$C_{LF} = C_{L\alpha F}\alpha_F + \Delta^i C_{L\alpha F}\alpha_N$$

where the static derivatives are

$$C_{L\alpha F} = \left(\frac{\partial C_L}{\partial \alpha}\right)_F \; ; \; \Delta^i C_{L\alpha_F} = \left(\frac{\partial \Delta^i C_L}{\partial \alpha}\right)_F$$

Mathematically Eq. (2) has the same form as the tail lift in the down wash field of a conventional airplane. The induced lift derivative $\Delta^i C_{L\alpha_F}$ can be determined by measuring the flare lift in attached flow with a slender nose as well as in the separated flow from the blunt nose. $\Delta^i C_{L\alpha_F}$ has then the following limits (See Fig. 2):

$$\left(\frac{\partial C_{LF}}{\partial \alpha}\right)_{SEP.\ FLOW} - \left(\frac{\partial C_{LF}}{\partial \alpha}\right)_{ATT.\ FLOW} < \Delta^i C_{L\alpha_F} < \left(\frac{\partial C_{LF}}{\partial \alpha}\right)_{SEP.\ FLOW}$$

Photographs of wakes for a typical test shape are shown in Fig. 3. Values of the ratio $\Delta^i C_{L\alpha_F}/(C_{L\alpha_F})_{ATT.\ FLOW}$ exceeding 6 were obtained from the data in (2). This large induced lift has been attributed to the large velocity (kinetic energy) gradients through the wake from the nose.

The most distinctive feature of Eq. (2) is: induced lift at the flare, $\Delta^i L_F$, is independent of the local angle of attack at the flare, α_F, and is dependent only upon the angle of attack at the nose, α_N. In other words, the induced lift at the flare at time t is dependent upon the angle of attack produced upstream at time $t-\Delta t$. In the static, stationary case the flow fields produced at time t and $t-\Delta t$ are identical. In the dynamic, non-stationary case, however, the flow fields will be different and the time lag, $\Delta t = b/U$, will appear explicitly in the equation of motion.

Aerodynamic Forces in Non-Stationary Flow

The effects of time lag, Δt, in a non-stationary flow field can be demonstrated easily for a rigid body undergoing pitching and plunging motion. For this demonstration we shall limit ourselves to the representation of the lift force on the flare as expressed by Eq. (2), omitting aerodynamic derivatives which are negligibly small. For simplicity, the lift at the nose is also omitted. Consider the force on the flare at time

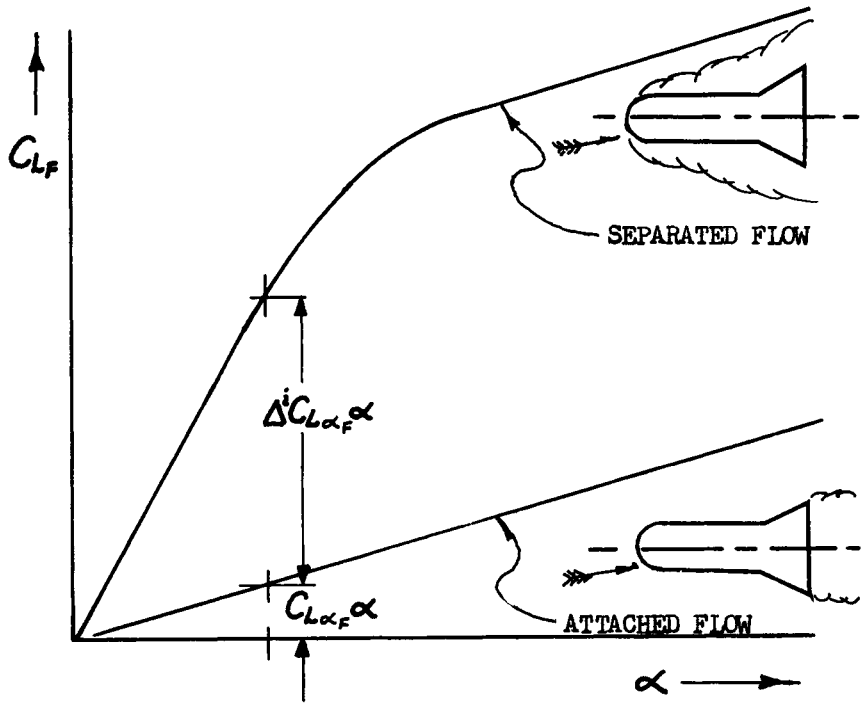

Fig. 2. Flare Lift of a Blunt Body of Revolution.

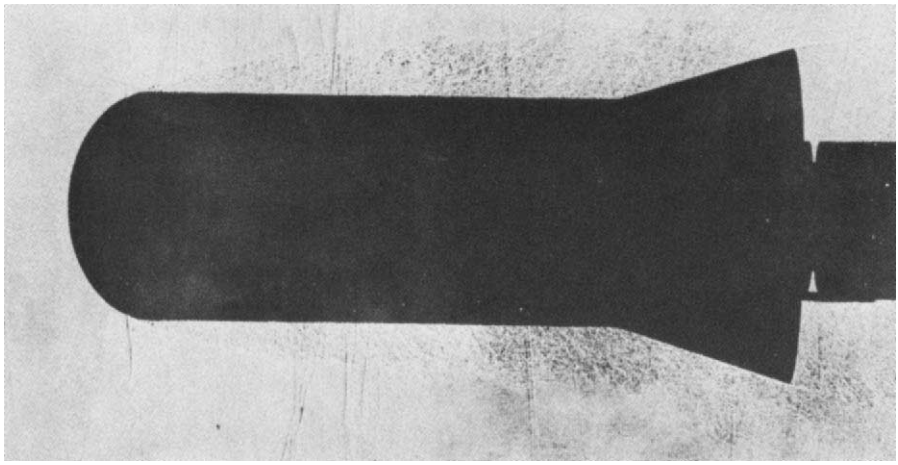

$\alpha = 0$

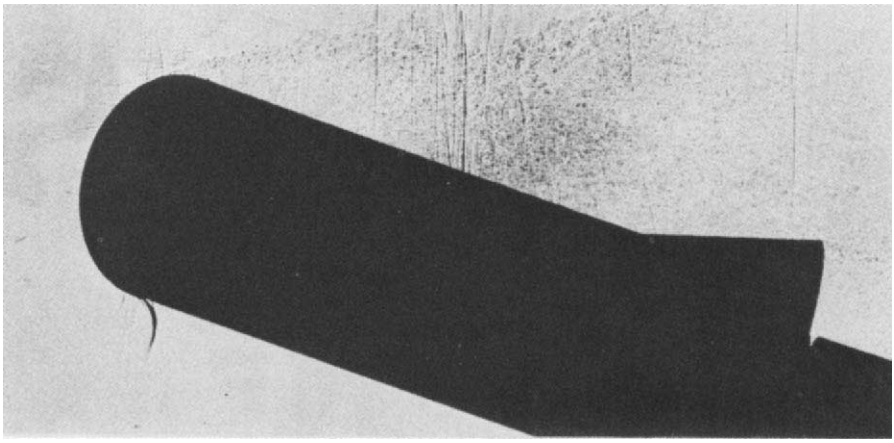

$\alpha > 0$

Fig. 3. Wakes of Separated Flow for a Blunt, Flared Body of Revolution.

t. The vehicle is executing plunging, $z(t)$, and pitching, $\theta(t)$, as shown in Fig. 4. The vehicle is shown at two instants of time. At $t-\Delta t$ the nose is at angle of attack

$$\alpha_N(t-\Delta t) = \frac{\dot{z}(t-\Delta t)}{U} + \theta(t-\Delta t) - x_N \frac{\dot{\theta}(t-\Delta t)}{U}$$

At an interval of time later, $\Delta t = b/U$, the flare has traversed the distance b, so that at time t, the flare is now in the flow field generated by the nose at time $t-\Delta t$. The transverse displacement, d, will be neglected assuming small displacements. Thus, when applied to a dynamic analysis, Eq. (2) becomes

$$L_F(t) = \frac{\rho U^2}{2} S \left\{ C_{L\alpha_F} \left[\frac{\dot{z}(t)}{U} + \theta(t) - \frac{x_F}{U}\dot{\theta}(t) \right] + \Delta^i C_{L\alpha_F} \left[\frac{\dot{z}(t-\Delta t)}{U} + \theta(t-\Delta t) - \frac{x_N}{U}\dot{\theta}(t-\Delta t) \right] \right\} \quad (3)$$

Eq. (3) is seen to consist of two parts similar to Eq. (2). The first part is in phase with the motion of the flare. The second part is induced by the motion of the nose at a previous instant, $t-\Delta t$; i.e., the force is out of phase with respect to the instantaneous motion of the flare by the time lag, $\Delta t = b/U$. Both forces as expressed in Eq. (3) are quasi-steady forces; that is, they are independent of the history of the motion prior to time t and $t-\Delta t$, respectively. For complete rigor, both of these forces should be calculated in terms of response to the corresponding angle of attack histories. Unfortunately, no theory known to the authors will account for the complete flow separation at the nose and the response can not be calculated analytically. The quasi-steady portion of the response can, however, be determined from static wind tunnel tests, and from the limited amount of data available for blunt-nose, flared bodies of revolution, it appears that the difference between the quasi-steady response and the actual response is small for low values of reduced frequency, $c\omega/U$. The data of (2) show the static value of $\Delta^i C_{L\alpha_F}$ to be virtually identical with the value obtained from forced oscillation tests for values of reduced frequency $c\omega/U$ up to 0.1. Thus, the forces described by Eq. (3) may be assumed to be sufficiently accurate for the lower bending frequencies. Moreover, from energy considerations with finite structural damping, the higher bending modes become less important in determining a critical speed range and may be neglected.

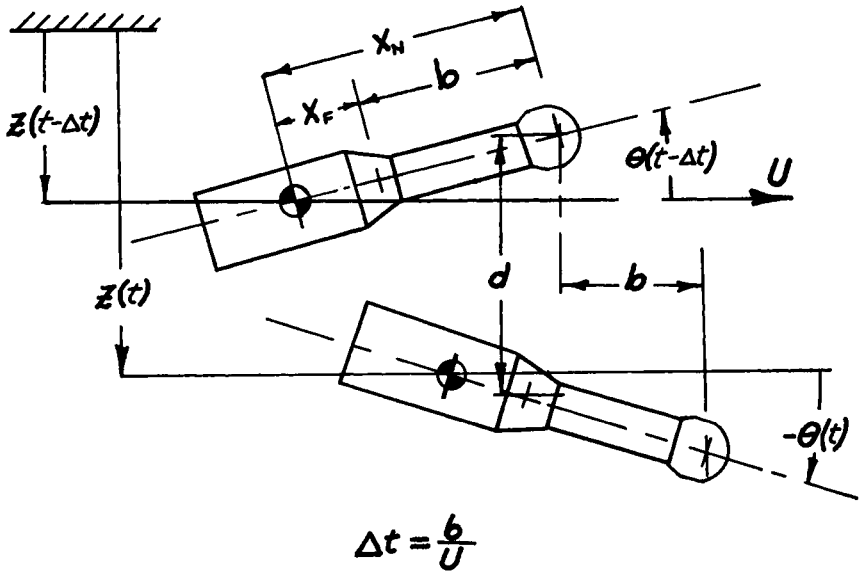

Fig. 4. Position of Vehicle at Two Instants of Time (Note: The translatory displacement, d , is greatly exaggerated in the sketch.)

Dynamic Analysis

In the analysis to follow, these assumptions are made:

1. The effect of drag is negligible.
2. The missile is moving with constant speed through air of constant density.
3. Linearized methods can be used.
4. The oscillations are slow, i.e., of low reduced frequency so that quasi-steady theory is valid.
5. The lift distribution over the missile can be represented by discrete forces.
6. The lift forces consist of two components:
   (a) local lift, i.e., lift due to local motion
   (b) induced lift, i.e., lift induced by the wake created at the nose.

With these assumptions the lift dependent upon local motion is simply

$$L(x,t) = \frac{\rho U^2}{2} S C_{L\alpha}(x) \tilde{\alpha}(x,t) \tag{4}$$

where $\tilde{\alpha}(x,t) = \theta(x,t) + \frac{\dot{z}(x,t)}{U}$

$\theta(x,t)$ = local geometric angle of attack
$\dot{z}(x,t)$ = local total translatory velocity

The induced flare lift is created by the wake generated at the nose at time $t-\Delta t$ and can be written

$$\Delta^i L(x_N-b,t) = \frac{\rho U^2}{2} S \Delta^i C_{L\alpha}(x_N-b) \tilde{\alpha}(x_N, t-\Delta t) \tag{5}$$

where $\tilde{\alpha}(x_N, t-\Delta t) = \theta(x_N, t-\Delta t) + \frac{\dot{z}(x_N, t-\Delta t)}{U}$

The term $\Delta^i C_{L\alpha}(x_N-b)$ is the induced flare force derivative $\Delta^i C_{L\alpha_F}$ measured statically provided that:

1. The displacement of the flare is small enough so that $\Delta^i C_{L\alpha_F}$ remains constant for the translatory displacement $z(x_N) - z(x_N-b)$.
2. The wave length of a disturbance in the flow field generated at the nose is large compared to the radial and axial extent of the flare. This implies that the reduced frequency, ω/U, of the oscillatory displacement must be small.

Elastic Oscillations

The stability of a missile performing elastic bending oscillations is analyzed, assuming that the "rigid body missile" is undisturbed. The local pitching and plunging of any point

on the axis are then produced only by elastic deflections. The elastic deflection $\delta(x)$ and the slope $\delta'(x) = \partial\delta(x)/\partial x$ at any station along the body may be represented by the series

$$\delta(x,t) = \sum_{i=1}^{\infty} q_{fi}(t) F_i(x)$$
$$\delta'(x,t) = \sum_{i=1}^{\infty} q_{fi}(t) F_i'(x) \tag{6}$$

where $q_{fi}(t)$ are the normal coordinates, $F_i(x)$ are the normal modes, and $F_i'(x)$ are the normal mode slopes.

As the translatory displacement and angle of attack are $z(x,t) = \delta(x,t)$; $\theta(x,t) = -\delta'(x,t)$, Eqs. (4) through (6) yield the following expressions for the lift forces.

Local lift:

$$L(x,t) = \frac{\rho U^2}{2} S C_{L\alpha}(x) \sum_{i=1}^{\infty} \left\{ -q_{fi}(t) F_i'(x) + \frac{\dot{q}_{fi}(t)}{U} F_i(x) \right\} \tag{7}$$

Induced lift:

$$\Delta^i L(x_N - b(x), t) = \frac{\rho U^2}{2} S \Delta^i C_{L\alpha}(x_N - b(x)) \sum_{i=1}^{\infty} \left\{ -q_{fi}(t-\Delta t) F_i'(x_N) + \frac{\dot{q}_{fi}(t-\Delta t)}{U} F_i(x_N) \right\} . \tag{8}$$

Δt is the time required for a disturbance from the nose to reach station $x_N - b(x)$. If the disturbance is assumed to travel downstream with the free-stream velocity, U, the time lag Δt becomes simply

$$\Delta t = \frac{b(x)}{U} \tag{9}$$

The equations of motion can be written as

$$\tilde{m}_i \ddot{q}_{fj}(t) + \tilde{m}_i \{1 + ig\} \omega_i^2 q_j(t) = P_j \tag{10}$$

or alternatively

$$\tilde{m}_i \ddot{q}_j(t) + \tilde{m}_i 2\zeta\omega_i \dot{q}_j(t) + \tilde{m}_i \omega_i^2 q_j(t) = P_j \qquad (10)$$ Cont'd

where

$$P_j = -\sum_{body} L_{i,j}(x,t) F_j(x) - \sum_{body} \Delta^i L_{i,j}(x_N - b(x), t) F_j(x_N - b(x))$$

$\tilde{m}_i$ = generalized mass

g or 2ζ = structural damping coefficient

ω_i = natural free-free bending frequency

P_j = generalized force

P_j is obtained from the virtual work done by the lift forces over the missile. Subscripts i and j designate row and column elements. Since the q_i are normal coordinates, they are not coupled elastically or inertially. Neglecting the aerodynamic coupling between the modes in Eq. (10), the subscripts (i) and (j) may be dropped and the equation of motion for an arbitrary bending mode becomes

$$\ddot{q}(t) + \{1 + ig\}\omega^2 q(t) = -\frac{\rho U^2 S}{2\tilde{m}}\left\{\sum_{body} C_{L\alpha}(x) F(x)\left[-F'(x) q(t) + \frac{F(x)}{U}\dot{q}(t)\right] + \sum_{body} \Delta^i C_{L\alpha}(x_N - b(x)) F(x_N - b(x))\left[-F'(x_N) q(t-\Delta t) + \frac{F(x_N)}{U}\dot{q}(t-\Delta t)\right]\right\}. \qquad (11)$$

In what follows, Eq. (11) is simplified without loss of generality by neglecting:

1. All local lift forces over the body except the local lift at the nose.
2. All induced lift forces over the body except the lift induced at the flare.
3. All control system forces.

With these assumptions, Eq. (11) is reduced to

$$\ddot{q}(t) + \frac{B}{U} C_{L\alpha}(x_N)\dot{q}(t) + \left[\{1+ig\}\omega^2 - B\frac{F'(x_N)}{F(x_N)} C_{L\alpha}(x_N)\right] q(t) + B\frac{F(x_N - b)}{F(x_N)} \Delta^i C_{L\alpha}(x_N - b)\left[\frac{\dot{q}(t-\Delta t)}{U} - \frac{F'(x_N)}{F(x_N)} q(t-\Delta t)\right] = 0 \qquad (12)$$

where

$$B = \rho\frac{U^2}{2} S \left\{F(x_N)\right\}^2$$

The solution to Eq. (12) may be cast in the complex form

$$q_\beta(t) = q_{\beta_0} \exp(i\nu t)$$

where

q_{β_0} = amplitude

ν = frequency

so that

$$q_\beta(t-\tfrac{b}{U}) = q_\beta(t)\cos\left(\frac{b\nu}{U}\right) - \frac{\dot{q}_\beta(t)}{\nu}\sin\left(\frac{b\nu}{U}\right)$$

and

$$\dot{q}_\beta(t-\tfrac{b}{U}) = \dot{q}_\beta(t)\cos\left(\frac{b\nu}{U}\right) + \nu q_\beta(t)\sin\left(\frac{b\nu}{U}\right)$$

Substituting these relations in Eq. (12), yields a familiar second order differential equation in $q_\beta(t)$.

$$\ddot{q}_\beta(t) + \frac{B}{U}\left\{\epsilon + C_{L_\alpha}(x_N) + \Delta' C_{L_\alpha}(x_N - b)\frac{F(x_N-b)}{F(x_N)}\frac{\sqrt{1+\sigma^2}}{\sigma}\sin\left(\frac{\nu b}{U} + \arctan\sigma\right)\right\}\dot{q}_\beta(t)$$

$$+\left\{\omega^2 - \frac{BF'(x_N)}{F(x_N)} + \Delta' C_{L_\alpha}(x_N - b)\sqrt{1+\sigma^2}\cos\left(\frac{\nu b}{U} + \arctan\sigma\right)\right\}q_\beta(t) = 0 \qquad (13)$$

where

$$\sigma = \frac{\nu}{U}\frac{F(x_N)}{F'(x_N)} \; ; \qquad \epsilon = g\frac{\omega^2 U}{\nu B}$$

In general, the structural stiffness is much larger than the aerodynamic stiffness and ν will be closed to ω. Thus, the

criterion for damped oscillation becomes

$$C_{L\alpha}(x_N) + \epsilon + \Delta C_{L\alpha}(x_N - b)\frac{F(x_N - b)}{F(x_N)}\frac{\sqrt{1+\sigma^2}}{\sigma}\sin\left(\frac{b\omega}{U} + \arctan\sigma\right) > 0 \quad (14)$$

where $\sigma = \frac{\omega}{U}\frac{F(x_N)}{F'(x_N)}$; $\epsilon = g\frac{\omega U}{B}$

Rearranging Eq. (14) to

$$\frac{\Delta C_{L\alpha}(x_N - b)\frac{F(x_N - b)}{F(x_N)}}{C_{L\alpha}(x_N) + \epsilon} \geq -\frac{\sigma}{\sqrt{1+\sigma^2}}\cos\left(\frac{b\omega}{U} + \arctan\sigma\right) \quad (15)$$

we see that the right hand side forms a stability boundary which is a function of the reduced frequency $b\omega/U$. The amplitude of the cosec function is modulated by the quantity $\sigma/\sqrt{1+\sigma^2}$ which is also a function of $b\omega/U$ since

$$\sigma = \frac{\omega}{U}\frac{F(x_N)}{F'(x_N)} = \left(\frac{b\omega}{U}\right)\left(\frac{1}{bF'(x_N)/F(x_N)}\right)$$

The quantity, $bF'(x_N)/F(x_N)$, in this relation is a fixed quantity for a given mode. Therefore, the right hand side of Eq. (15) may be visualized as a stability boundary for one bending mode of a specific vehicle throughout the speed range defined by the reduced frequency, $b\omega/U$. This is illustrated in Fig.5 for a typical case where $bF'(x_N)/F(x_N) = 1.5$.

In a typical structure the value of σ will change only slightly from one bending mode to another. Hence, Fig. 5 may also be visualized as a stability boundary for all bending modes of a specific vehicle moving at constant velocity.

In either case, as $b\omega/U$ is varied from zero to infinity, the modulator, $\sigma/\sqrt{1+\sigma^2}$, in Eq. (15) varies from zero to unity. Thus, the modulator tends to distort the cosecant function for low values of $b\omega/U$ and the boundary becomes indeterminate at zero. Since it is possible that a first bending mode may lie within this region, it is of interest to examine the stability boundary here. This can be done by reformulating Eq. (15); that is, by expanding $\cos(b\omega/U)$ and $\sin(b\omega/U)$ to yield

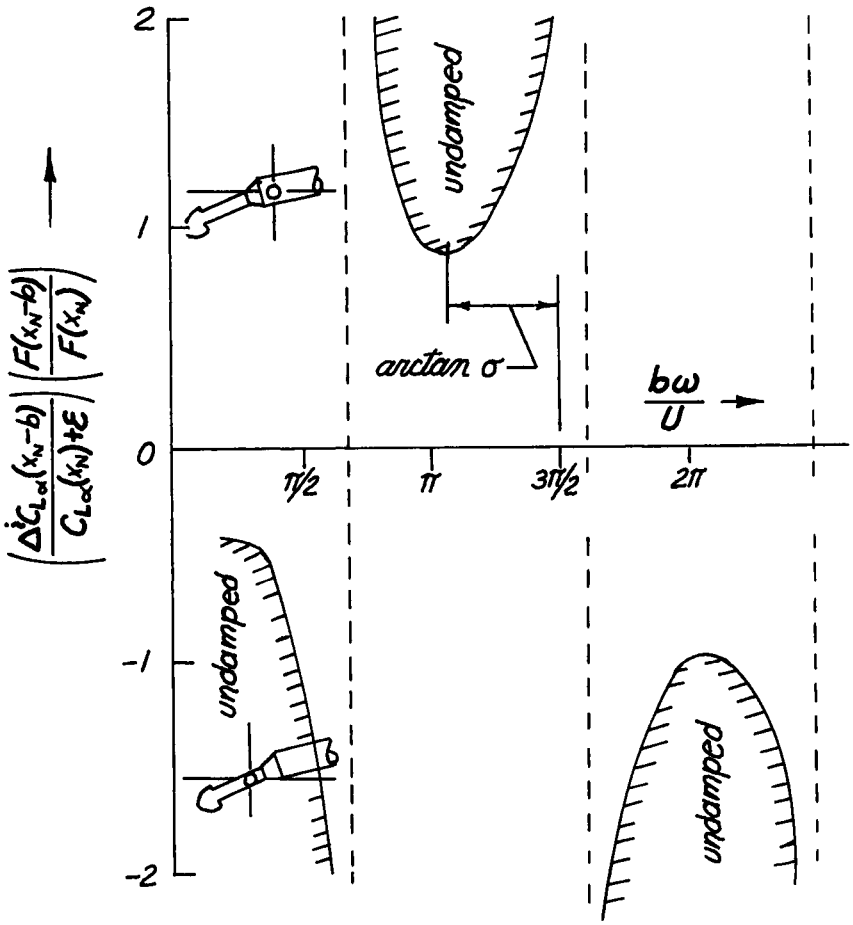

Fig. 5. (a) Stability Boundary of an Arbitrary Bending Mode Throughout Speed Range, $b\omega/U$, for a Specific Vehicle.

(b) Stability Boundary of All Modes for a Specific Vehicle Moving at Constant Speed.

$$\frac{\Delta' C_{L\alpha}(x_N - b)\frac{F(x_N - b)}{F(x_N)}}{C_{L\alpha}(x_N) + \epsilon} > -\frac{1}{1 + \frac{bF'(x_N)}{F(x_N)} - \frac{1}{2}\left(1 + \frac{b}{3}\frac{F'(x_N)}{F(x_N)}\left(\frac{b\omega}{U}\right)^2 + \cdots\right)} \quad (16)$$

Here we see that the reduced frequency, $b\omega/U$, has only a second order effect upon the stability boundary represented by the right hand side of Eq. (15). The boundary is plotted for values of $b\omega/U$ up to .7 in Fig. 6 for the same vehicle assumed for Fig. 5.

Discussion of Stability Criteria

The stability criterion provided by Eq. (15) is shown graphically in Fig. 5. The meaning of the various branches of cosecant ($b\omega/U + \arctan \sigma$) may be demonstrated by considering the net gain of energy per cycle from a linear second order system of the form

$$m\ddot{q}_f(t) + D\dot{q}_f(t) + Kq_f(t) = 0 \quad (17)$$

The net gain of energy can be computed by integrating the work done by the forces in Eq. (17) in completing a cycle. If the system is performing pure harmonic oscillation of amplitude q_{f_0}, and frequency ω, the work done is

$$W = -\pi q_{f_0}^2 \omega D \quad (18)$$

Hence, the work done per cycle is proportional to the coefficient for $\dot{q}_f(t)$ in Eq. (13) and is of opposite sign. Applying the result to Eq. (18), we see that the work done per unit mass is

Work done by nose lift: $-\pi q_{f_0}^2 \omega \frac{B}{U} C_{L\alpha}(x_N)$

Work done by structural damping: $-\pi q_{f_0}^2 \omega^2 g$

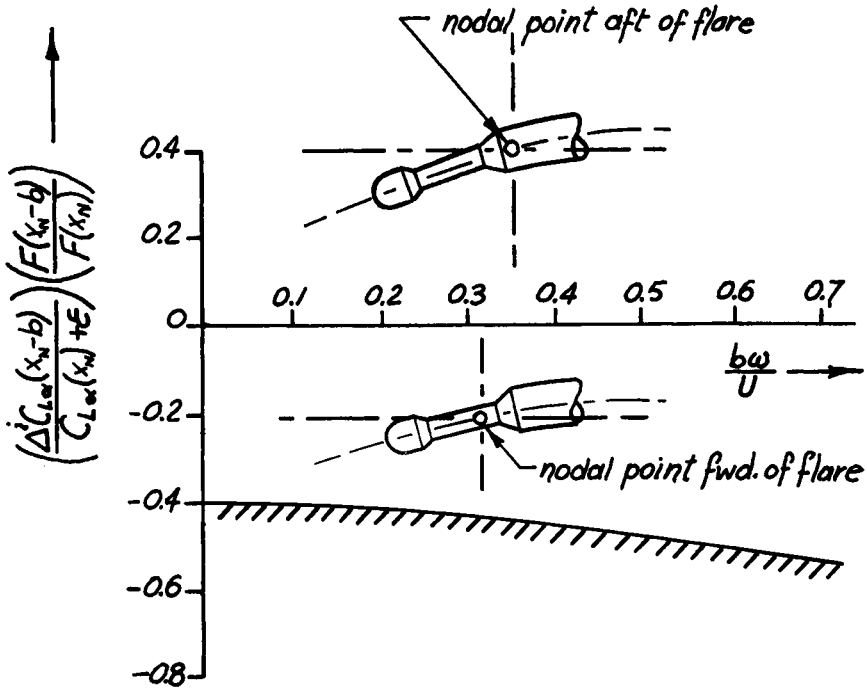

Fig. 6. Stability Boundary of an Arbitrary Bending Mode for a Specific Vehicle at Low Reduced Frequency.

Work done by induced flare lift:

$$-\pi q_{\infty}^2 \omega \frac{B\sqrt{1+\sigma^2}}{U\sigma} \Delta C_{L\alpha}(x_N-b)\frac{F(x_N-b)}{F(x_N)} \sin\left(\frac{b\omega}{U}+\arctan\sigma\right)$$

We see that the work done by the lift at the nose is proportional to $-C_{L\alpha}(x_N)$ and is negative for positive nose lift.

The work done by structural damping is also negative and represents energy dissipated by the structure. The ratio of this quantity to the work done by the aerodynamic forces is proportional to the natural bending frequency. Because of this, we can expect the higher modes to be more difficult to excite.

The work done by the induced lift at the flare is proportional to

$$-\frac{F(x_N-b)}{F(x_N)} \sin\left(\frac{b\omega}{U}+\arctan\sigma\right)$$

and the coefficient of this quantity is positive, provided that $\Delta C_{L\alpha}(x_N-b) > 0$. Hence, positive work is done by the force; i.e., energy is extracted from the air stream, when the product of $F(x_N-b)/F(x_N)$ and the sine function is negative. That has a very simple physical meaning in Fig. 5; namely, all the negative branches of cosecant are stability boundaries for an odd number on nodal points between the nose and the flare. Again, the positive branches of cosecant ($b\omega/U+\arctan\sigma$) are stability boundaries for an even number (including zero) of nodal points between the nose and the flare. For example, in a typical configuration, the first two bending modes may contain one nodal point ahead of the flare and as a consequence stability boundaries would be defined in the region $0<\arg(\operatorname{cosec})<\pi$. The third and fourth bending modes could then contain two (but not zero) nodal points ahead of the flare, and so the stability boundary would be provided by the positive branch for $\pi<\arg(\operatorname{cosec})<2\pi$ and so on for the higher modes. When the bending modes have one nodal point forward of the flare, only the first branch of Fig. 5 needs to be examined. Or, in the case of low values of $b\omega/U$, Fig. 6 (Eq. (16)) should be used.

In (2) it is shown that the critical ratio of induced flare lift to nose lift for a blunt-nose flared re-entry body is determined by the position of the c.g. of the body along its longitudinal axis. Eq. (16) yields a similar result when structural damping, ε , is set equal to zero. The ordinate of Fig. 6 then becomes

$$\frac{\Delta' C_{L\alpha}(x_N-b)}{C_{L\alpha}(x_N)} \cdot \frac{F(x_N-b)}{F(x_N)}$$

The similarity between the single degree of freedom stability of the low frequency bending modes and the stability in pitch of the rigid re-entry body from (2) is shown by the following analogy.

Elastic Missile	Rigid Re-entry Body
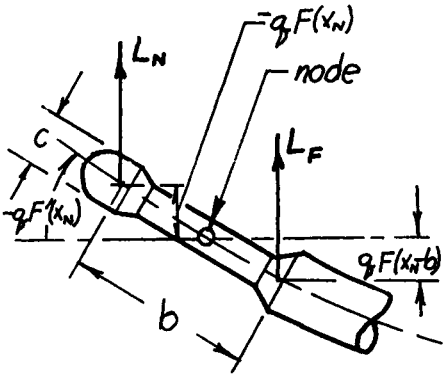	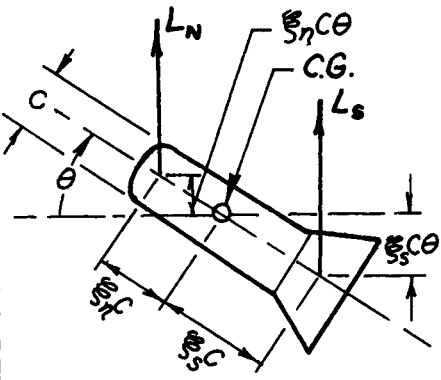
For stability when $\left(\frac{b\omega}{U}\right)^2 \ll 1$	For stability when $\left(\left\{\xi_\eta + \xi_s\right\}\frac{C\omega}{U}\right)^2 \ll 1$
$\frac{F(x_N-b)}{F(x_N)} \frac{\Delta' C_{L\alpha}(x_N-b)}{C_{L\alpha}(x_N)} > -\frac{1}{1+\frac{bF'(x_N)}{F(x_N)}}$	$-\frac{\xi_s}{\xi_\eta} \frac{\Delta' C_{L\alpha_s}}{C_{L\alpha_\eta}} > -\frac{1}{1+\frac{\xi_s+\xi_\eta}{\xi_\eta}}$

The significance of this analogy is: The stability of the elastic missile can be determined by wind tunnel tests with a rigid model.

The purpose of this paper is to demonstrate one of many possible mechanisms for unstable bending oscillation of "hammerhead" missiles. The mechanism shown is one, however, that may easily be overlooked for the following reasons: The blunt payload by itself (in absence of flare) may contribute to dynamic stability and so may the flare in presence of a less

blunt nose, yet the combination of a blunt payload and a flared interstage may well be dynamically unstable. The analysis is restricted to small amplitudes and aerodynamic characteristics for which linearized methods could be applied, and is simplified further by use of various approximations, some of which could be easily removed. For pure elastic oscillations the amplitudes will usually be small enough to satisfy the condition required for linear aerodynamic forces and the analysis can then be extended to coupled elastic modes. However, in considering coupling with rigid body motion, non-linear amplitude effects may have to be considered. This can to a certain extent be accomplished by considering the work done by the aerodynamic forces, as is done in (2) and (3).

Conclusions

The aerodynamic forces acting on a missile whose composite shape combines a blunt nose with a flared interstage may cause self-excited bending oscillations throughout a considerable range of high subsonic and transonic speeds.

In order to determine if a particular configuration is prone to experience this kind of instability, it is essential to obtain static wind tunnel measurements of lift at the nose and the flare. If possible, the static data should be confirmed by dynamic tests (such as forced-oscillation of a rigid model) as there is at present no satisfactory analytic method available to predict the force induced in a wake of separated flow.

The destabilizing effect of the induced flare lift can be reduced by the following steps.

1. Reducing the induced flare lift by
   (a) Modifying the nose shape
   (b) Modifying the flare.
2. Modifying the structure so that the flare is closer to or forward of the nodal point for the lower bending modes.

These conclusions are based upon the assumption that aerodynamic coupling between the elastic modes is negligible. This appears to be a valid assumption for a wide range of practical cases.

References

1. Coe, Charles F., "Steady and Fluctuating Pressure at Transonic Speeds on Two Space Vehicle Payload Shapes", NASA TM X503, March 1961.

2. Ericsson, L-E., "Relation Between Static and Dynamic Characteristics for a Slowly Oscillating Blunt Re-entry Body with Non-Linear Amplitude Effects, Part I, Pitch Oscillation Around a Fixed Axis", LMSD TM 53-14-100, April 1961, Confidential.

3. Ericsson, L-E., "Relation Between Static and Dynamic Characteristics for a Slowly Oscillating Blunt Re-entry Body with Non-Linear Amplitude Effects, Part II, Planar Motion-Pitch Oscillation and Translation", LMSD/DP/M-TM-24, April 1961.